Proceedings of the 46th International Conference on Electron, Ion and Photon Beam Technology and Nanofabrication, Anaheim, May 2002, J. Vac. Sci. Technol. B, in press

Single Ion Implantation for Solid State Quantum Computer Development

T. Schenkel[#, 1], A. Persaud[1], S. J. Park[1], , J. Meijer[1,*], J. R. Kingsley[2], J. W. McDonald[3], J. P. Holder[3], J. Bokor[1,4] and D. H. Schneider[3]
[1]E. O. Lawrence Berkeley National Laboratory, Berkeley, CA 94720
[2]Charles Evans and Associates, Sunnyvale, CA 94086
[3]Lawrence Livermore National Laboratory, Livermore, CA 94550
[4]Department of Electrical Engineering and Computer Sciences, University of California, Berkeley, CA 94720

Several solid state quantum computer schemes are based on the manipulation of electron and/or nuclear spins of single ^{31}P atoms in a solid matrix. The fabrication of qubit arrays requires the placement of individual atoms with nanometer precision and high efficiency. We describe the status of our development of a low energy, single ion implantation scheme for $^{31}P^{q+}$ ions. High ion charge states enable registration of single ion impacts with unity efficiency through the detection of secondary electrons. Imaging contrast in secondary electron emission allows alignment of the implantation and integration with consecutive lithography steps. Critical issues of process integration and resolution limiting factors are discussed.

1. Introduction

The finding of quantum algorithms for factoring and database search that show exponential and quadratic speedup, respectively, compared to classical codes has sparked a rapidly growing interest in the physical realization of quantum computers [1]. Quantum computers will have to be scaled to a few thousand qubits in order to harvest the power of quantum algorithms. The problem of scalability favors conceptual approaches in the solid state, while important proof-of-principle demonstrations are being achieved with nuclear magnetic resonance (NMR), ion and atom trap techniques that might not be scalable to a few thousand qubits. In several solid state schemes, quantum computation is realized through the manipulation of electron and/or nuclear spins of ^{31}P atoms [2-5]. In Kane's proposal, NMR techniques are used together with electrical gates to address and manipulate nuclear spins of ^{31}P atoms in silicon through the hyperfine interaction with bound donor electrons. Nuclear spins are attractive quantum memories, because they can be manipulated selectively through control of the hyperfine interaction, but are also very well isolated from their environment. The interaction of neighboring ^{31}P qubits is mediated through the exchange interaction, where the wave function overlap of donor electrons is controlled with a second set of gates. In relaxed silicon, this requirement fixes the qubit spacing to about 15 to 20 nm for an exchange interaction strength in the 0.1 meV range. Virjen et al. suggested to use only the electron spins and exchange interaction, and proposed to employ silicon germanium hetero-structure engineering to design a solid host in which the Bohr radii of bound donor electrons are ten times larger than in unstrained silicon [4]. A similar relaxation of qubit spacing requirements is achieved when electrons in a 2D electron gas in the quantum Hall regime mediate the interaction of neighboring ^{31}P qubits which can then be spaced ~100 nm apart [5]. Koiller et al. have calculated the effect of donor spacing on the exchange coupling for a series of qubit hosts such as unstrained and strained silicon, and Si_xGe_y structures [6], and

[#] e-mail: T_Schenkel@LBL.gov

revealed pronounced oscillations of the coupling strength as a function of the in plane donor distance on an Ångstrom length scale. The difficulty in controlling donor positions to such a degree might favor "electron shuttling" rather than direct wave function overlap as a means to entangle neighboring donors [3].

This brief discussion is to illustrate that this is a rapidly evolving field where experimental tests of basic building blocks of solid state quantum computers are essential for validation of device schemes. A basic building block of the original Kane scheme is a set of ^{31}P atoms in silicon, aligned to gate and readout structures. There are two basic approaches to the fabrication of single atom arrays inside a solid [2]. In a "bottom up" manner, arrays of ^{31}P atoms can be deposited on a silicon surface though STM based hydrogen lithography [7, 8], followed by encapsulation, annealing and consecutive gate and readout fabrication. In the "top down" path, donor ions are implanted into the matrix by single ion implantation (SII) [9, 10]. Key issues in both approaches are the conservation of the single atom arrays structures during consecutive processing steps, especially when the dopant atoms have to be annealed to ensure electrical activation. In the following, we will discuss basic requirements for single ion implantation in the context of solid state quantum computer development, and then describe our SII scheme.

2. Requirements for single ion implantation

In an ideal single ion implanter, individual ions (of any element) are delivered into a controlled area on a wafer at a reasonable rate, each ion impact is registered, and the beam is turned off fast enough to prevent impact of the next ion before the sample has been moved to the next implant position. Direct write techniques such as sequential single ion implantation are generally too slow for mass production of IC components, but a rate of only a few ions per second suffices for the fabrication of test components of solid state quantum computers and devices with a few thousand qubits.

Control of the ion position is addressed in the ion optical column of the implanter [11]. Commercial focused ion beam systems can deliver pA currents of ions from liquid metal ion guns (mostly Ga^+ and In^+) with kinetic energies of tens to a hundred keV into beam spots with diameters of about 10 nm. The problem of single ion detection can be solved by detection of secondary electrons that are formed when the ion impinges on the target. In the bulk, projectiles transfer momentum to target electrons and form electron-hole pairs, which can be separated and collected in an applied electrical field. This is the principle of solid state detectors and ion beam induced charge collection (IBICC). Use of this technique requires that samples are prepared to function as detectors [9]. A fraction of the secondary electrons that are formed in the sample by the impinging ion are emitted into the vacuum and their detection allows for the registration of individual ion impacts. Kinetic electron emission results from the transfer of kinetic energy of projectiles to target electrons, and typical secondary electron yields from metals for $^{31}P^+$ ions are between one and two electrons per ion [12]. The yield scales roughly linear with the electronic energy loss, and drops below one for kinetic energies below about 15 keV for $^{31}P^+$ ions on aluminum. Shinada et al. have reported a 90% detection efficiency for P^{2+} at 60 keV in a single ion implantation setup [13]. In contrast to kinetic electron emission, potential electron emission stems from the deposition of potential energy of projectiles that is associated with their charge states [14]. Potential electron emission is largely independent of projectile velocity and *increases* slightly with decreasing impact velocity [14]. Higher secondary electron yields for slower projectiles result from the increased time available for above surface relaxation of transient "hollow atoms" [14] through Auger transitions.

The effective resolution, x_{eff}, in the formation of electrically active single dopant atom arrays is determined by the beam spot size, straggling of the implanted ion during slowdown in the target, and finally by diffusion in consecutive processing steps, such as annealing and gate oxide deposition. For a qubit spacing d (with d=10 to 20 nm in the original Kane proposal and d≈100 nm in several variations) the effective resolution in ^{31}P spacing should be a faction of d: $x_{eff} = \sqrt{x_{beam}^2 + x_{straggl}^2 + x_{diff}^2} < d$.

Straggling results from statistical energy loss processes during the slowdown of impinging ions and quantifies the spread of the longitudinal and lateral range profiles of the implanted ions in a solid. Straggling as estimated for ^{31}P in silicon with the SRIM code [15] amounts to 25 nm for a 50 keV implant with a 70 nm range. For an implantation energy of 10 keV the range is about 15 nm with a longitudinal straggle of 8 nm, and for 1 keV both range and straggling are only a couple of nm. Straggling thus sets a limit to the kinetic energy at which an effective implant resolution can be achieved. A consequence of reducing the impact energy is that single ion registration through detection of secondary electrons becomes impractical in a regime of kinetic electron emission because of the decrease of secondary electron yields. Use of highly charged projectiles avoids this limitation.

3. Experimental

A schematic of our single ion implantation setup is shown in Fig. 1. Beams of highly charged ^{31}P ions are extracted from the Electron Beam Ion Trap (EBIT) and reach the implant station after charge state analysis in a bending magnet [16]. The ion extraction potential can be varied from 2-25 kV and the implantation energy is defined in a deceleration lens system at the wafer. Ions are focused electrostatically and the beam spot size is limited by a collimating aperture. Secondary electrons are detected in an annular micro channel plate detector. The front plate of the detector can be biased positively with respect to the target for optimization of the secondary electron collection efficiency. Following the detection of an ion impact, the beam is turned off through the pulsing of an electrostatic element. Since the rate of ion transport through the last aperture is only a few tens of Hz, efficient beam blocking is easily achieved. Once the beam is blocked, the target is moved to the next implant position. The target stage is a piezo driven three axis nanopositioner with a lateral resolution of +/-1 nm and an x and y-range of 100 μm.

4. Results and discussion

The total number of charges extracted from EBIT at an electron beam current of 70 mA and an extraction potential of 6.5 kV is 0.5 to 1 nA. Typical beam currents after m/q analysis are 20 pA or 10^6 ions/s for $^{31}P^{12+}$ at 70 keV. Figure 2 shows the number of $^{31}P^{12+}$ ions transported through a set of apertures from 1 mm to 0.5 μm. A rate of 40 $^{31}P^{12+}$/s was achieved for the smallest aperture. A beam profile obtained by scanning a 25 μm aperture across the beam at a waist is shown in the insert. The emittance of the beam was determined to be 0.6 π mm mrad [17]. Here, phosphorous was introduced into the source from PF_3. The number of ions in the EBIT is limited by the space charge potential of the electron beam, and using PH_3 instead of PF_3 will at least double the available number of P^{q+} ions. Replacement of the beam line with 90° bending magnet with a more compact, axial optical column [17] with a Wien filter for charge separation will improve beam transport.

Collimators with aperture sizes as small as 30 nm have been fabricated by FIB drilling of silicon nitride membranes with a 30 keV Ga^+ beam. FIB drilling experiments indicate an aspect ratio limit of about 5:1, but the hole size is not independent of the aspect ratio for hole below a diameter of ~100 nm. Drilled areas can be imaged *in situ* in a dual beam FIB, but electron emission contrast does not reveal the presence of a hole through a thin aperture [10]. In Fig. 3.we show a TEM image of a 30 nm diameter hole in a 30 nm thick SiN membrane. In an alternative to FIB drilling, small spots can be defined in resist layer on thin membranes by electron beam, or scanning probe lithography, followed by dry etching for hole formation. Here, smaller hole diameters and larger aspect ratios can be achieved [18].

When $^{31}P^{q+}$ ions impinge on a wafer surface, their potential energy (2.5 keV for P^{12+}) is released, and about 15 to 20 secondary electrons are emitted [19]. Secondary electron yields depend on the target material, a fact that is commonly used for imaging during ion bombardment in focused ion beam systems. In Figure 4, we show pulse height distributions from secondary electrons for $^{31}P^{12+}$ impact on silicon (with native oxide) and copper surfaces. Contrast from potential electron emission allows alignment to markers that also show good contrast in electron beam lithography (EBL) [20]. Markers of thin SiO_2 and heavy metal films give contrast both in the implanter and EBL, and allow process integration of single ion implantation and EBL steps.

Next to beam spot size and range straggling, another challenge for qubit array formation is dopant diffusion during annealing. Annealing is required to incorporate the dopant atoms into the crystal lattice of the host material both in “top down” and “bottom up” approaches. Following ion implantation annealing also repairs the damage induced in the host crystal by the ions. A qubit spacing of 20 nm corresponds to a rather low area density of 2.5E11 $^{31}P/cm^2$. Diffusion of dopant atoms is defect mediated. Since the implant dose is low, dopants interact only with defects from a single collision cascade. Hence we expected that transient enhanced diffusion effects are minimal in this intrinsic implant regime [21]. In Fig. 5 we show magnetic sector secondary ion mass spectrometry (SIMS) depth profiles from low dose (2.5E11 cm^{-2}), low energy (5 keV) $^{31}P^{1+}$ implants in silicon with and without annealing. Samples were implanted randomly at an incident angle of 7° off the (100) axis. Rapid thermal annealing at 1000 °C was performed under N_2 atmosphere. The native oxide on wafers, which was present during implantation was removed prior to annealing, and was removed also from the control wafer. A thin oxide re-grows into the sample after exposure to ambient atmosphere. After annealing for 10 s, SIMS shows a slight broadening of the range profile, in agreement with SUPREM IV simulations [22]. C-V measurements for determination of electrical activation fractions are in progress.

Dopant loss in even a thin barrier or resist layer favors implantation into clean silicon, followed by annealing, and barrier layer deposition at low temperature to avoid parasitic diffusion. In the next step, gates and single electron transistor readout structures will be defined through electron beam lithography that is aligned to the implant positions. Clearly, alignment accuracy, and the distributions of atom positions will make for challenging yield management, but tests with qubit pairs are needed to assess placement accuracy requirements.

5. Conclusion

Low energy single ion implantation offers a route to the fabrication of ^{31}P arrays for tests of solid state quantum computer schemes. We discuss critical issues of single ion detection, and effective ion placement due to range straggling and dopant diffusion during rapid thermal annealing. Lowering the ion implant energy minimizes range straggling, but also makes beam transport more challenging. Improvements of the placement accuracy will allow integration with basic gate and readout structures and iterative tests of processing cycles.

Acknowledgments

We thank A. Liddle for discussions of SET integration; T. Radetic and E. Stach (NCEM, LBNL) for TEM and FIB support, and the staff of the Microlab at UC Berkeley. This work was supported by the National Security Agency and Advanced Research and Development Activity under Army Research Office contract number MOD707501, and by the U. S. DOE under Contract No. DE-AC03-76SF00098. Work at LLNL was performed under the auspices of the U. S. DOE under contract No. W-7405-ENG-48.

* permanent address: Department of Physics, Ruhr University Bochum, Germany

References

[1] for a recent review see: C. H. Bennett, and D. P. DiVincenzo, Nature 404, 247 (2000)
[2] R. G. Clark (editor) "Proceedings of the 1st International Conference on Experimental Implementation of Quantum Computation" (Rinton, Princeton, 2001)
[3] B. E. Kane, Nature 393, 133 (1998); A. J. Skinner, et al., quant-ph/0206159
[4] R. Vrijen et al., Phys. Rev. A 62, 12306 (2000)
[5] D. Mozyrsky, V. Privman, M. L. Glasser, Phys. Rev. Lett. 86, 5112 (2001)
[6] B. Koiller, X. D. Hu, S. Das Sarma, Phys. Rev. Lett. 88, 7902 (2002)
[7] J. L. O'Brien, et al., Phys. Rev. B 64, 1401 (2001); L. Oberbeck et al., cond-mat/0208355
[8] T. C. Shen et al., Appl. Phys. Lett. 80, 1580 (2002)
[9] D. N. Jamieson et al., in [2]; T. M. Buehler, et al., cond-mat/0208374
[10] T. Schenkel, et al., in "Quantum Dot Devices and Computing", J. A. Lott et al. (eds.) SPIE Proc. Vol. 4656, 10 (2002); cond-mat/0201549
[11] J. Orloff, Rev. Sci. Instr. 64, 1107 (1993)
[12] R. A. Baragiola, Nucl. Instr. Meth. B 78, 223 (1993)
[13] T. Shinada, et al., Jap. J. Appl. Phys. 38, 3419 (1999)
[14] A. Arnau, et al., Surf. Sci. Rep. 27, 117 (1997); T. Schenkel, et al. Prog. Surf. Sci. 61, 23 (1999)
[15] J. F. Ziegler, J. P. Biersack and U. Littmark, "The Stopping and Range of Ions in Solids" (Pergamon Press, New York, 1985)
[16] T. Schenkel, et al., Rev. Sci. Instr. 73, 663 (2002)
[17] R. E. Marrs, et al., Rev. Sci. Instr. 69, 204 (1998)
[18] I. Rangelow, T. Gotszalk, and T. Schenkel, to be published
[19] T. Schenkel et al., Nucl. Instr. and Meth. B 125, 153 (1997)
[20] J. Kedzierski, J. Bokor, and E. Anderson, J. Vac. Sci. Technol. B 17, 3244 (1999)

[21] N. Cowern, and C. Rafferty, MRS Bulletin 25, 39 (2000)
[22] R. W. Dutton, J. D. Plummer, Integrated Circuits Laboratory, Stanford Univ.

Figure captions:

Figure 1.: Schematic of the single ion implantation setup.

Figure 2: Intensity of the $^{31}P^{12+}$ beam as a function of aperture size. The insert shows the beam profile at a waist obtained with a 25 μm aperture.

Figure 3: TEM (magnification 150K) of a 30 nm wide test aperture in a 30 nm thick silicon nitride membrane from FIB drilling with a 30 keV Ga^+ beam. The surface structure is from a thin layer of Pt, which had been deposited to reduce charging.

Figure 4: Pulse height distributions of secondary electrons from $^{31}P^{12+}$ impacts on copper and silicon (with native oxide) samples from an annular MCP detector

Figure 5: Magnetic sector SIMS (CAMECA 4f) depth profiles of ^{31}P atoms (5 keV, 2.5E11 cm^{-2}) in silicon wafers as implanted (black) and after RTA at 1000º C for 10 s under N_2 atmosphere (red).

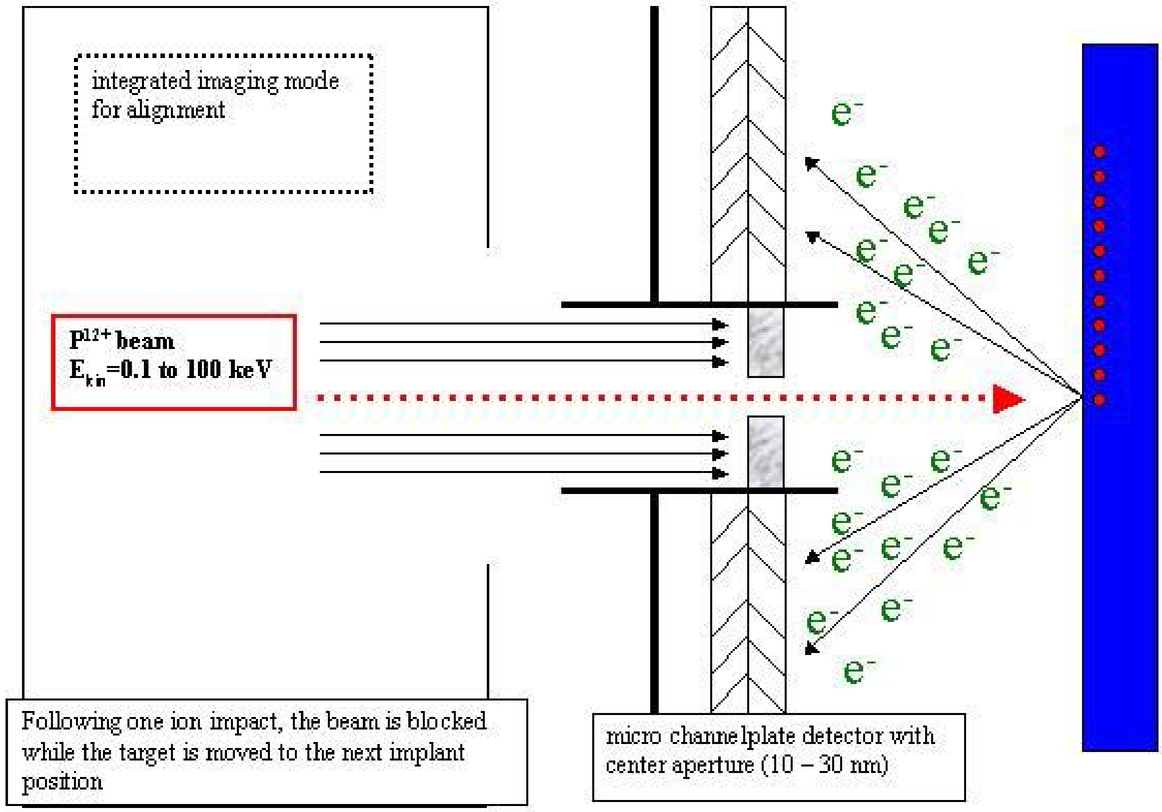
integrated imaging mode for alignment
P12+ beam
Ekin=0.1 to 100 keV
e-
Following one ion impact, the beam is blocked while the target is moved to the next implant position
micro channelplate detector with center aperture (10 – 30 nm)

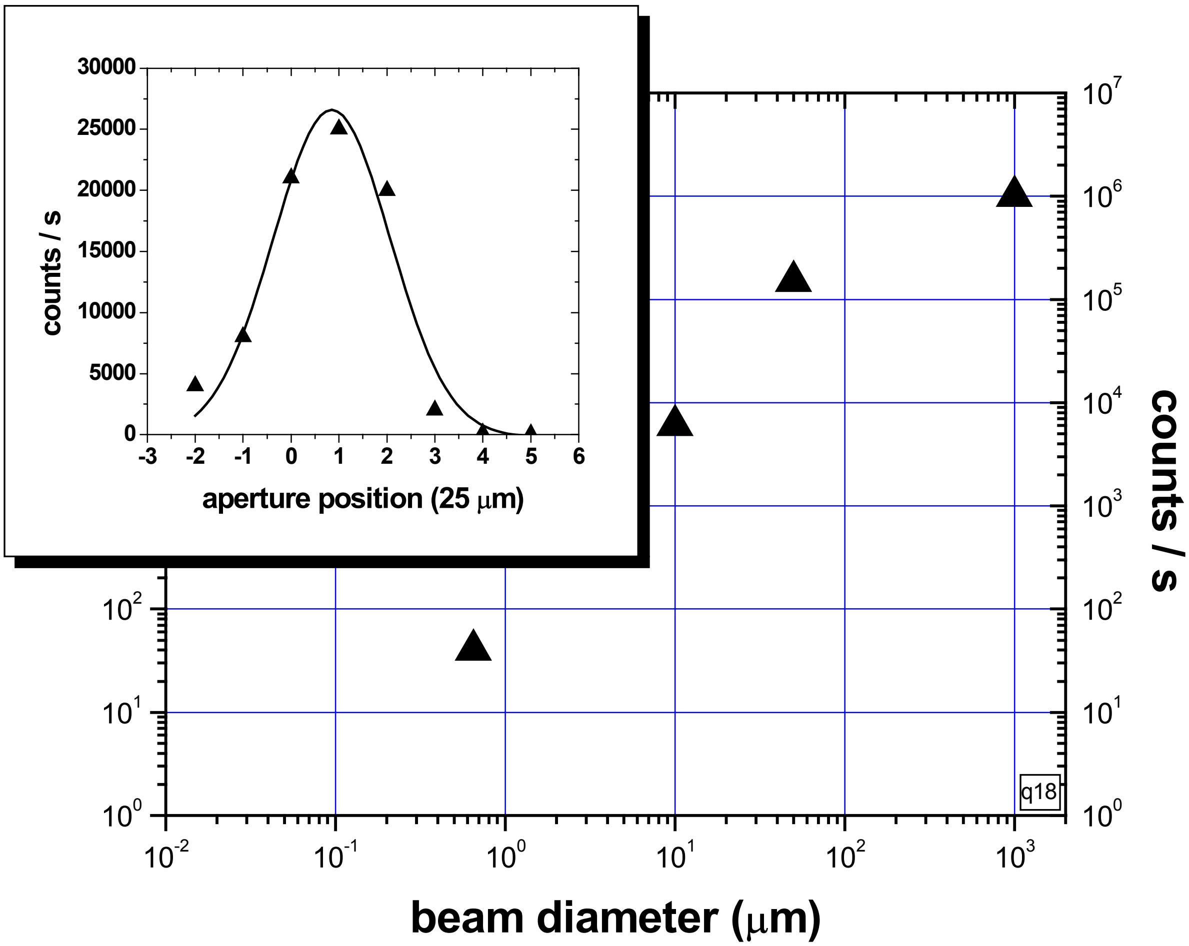
30000
25000
20000
15000
10000
5000
0
counts / s
-3 -2 -1 0 1 2 3 4 5 6
aperture position (25 μm)
10^7
10^6
10^5
10^4
10^3
10^2
10^1
10^0
counts / s
q18
10^-2 10^-1 10^0 10^1 10^2 10^3
beam diameter (μm)

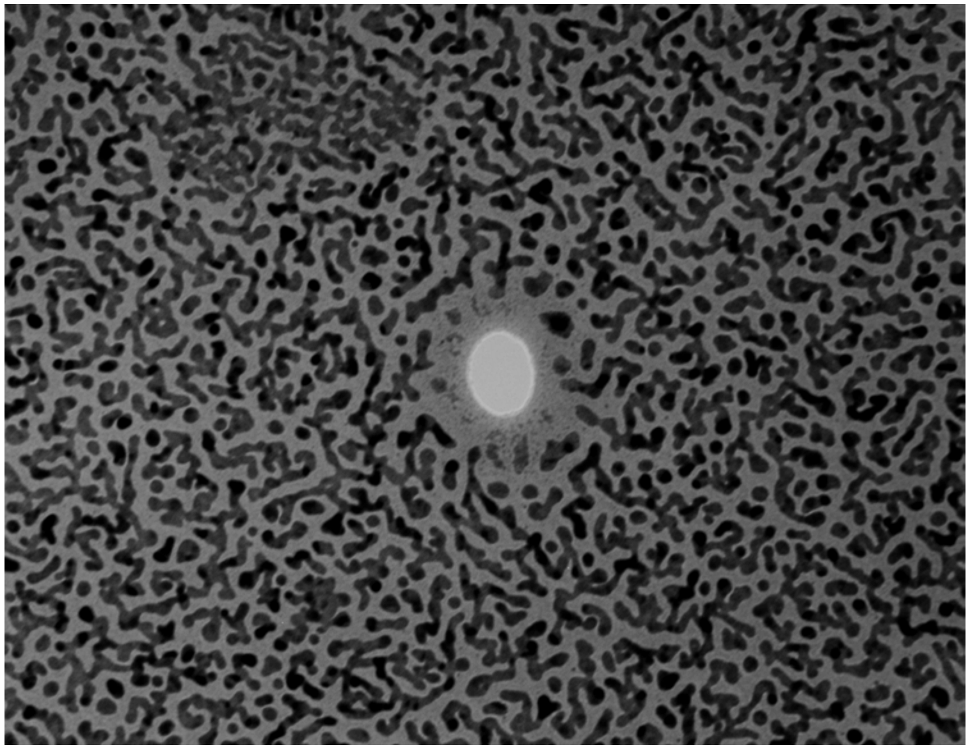

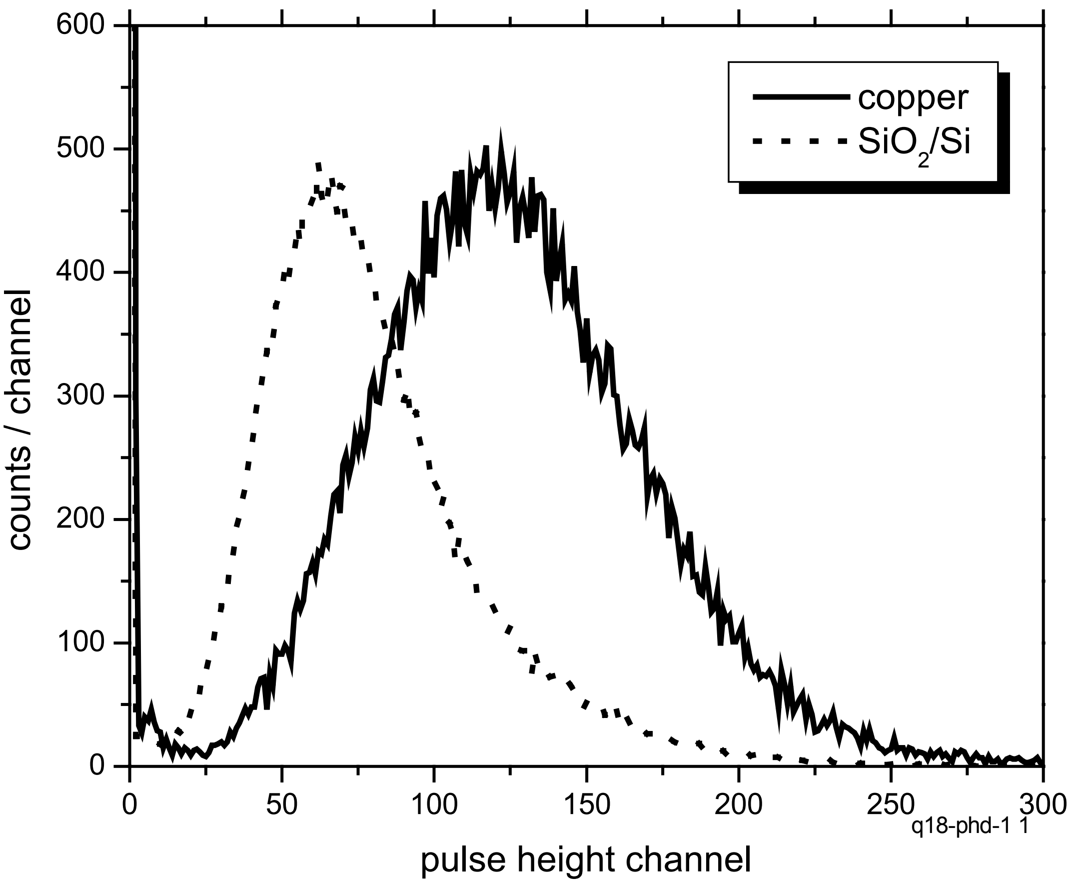

copper
SiO2/Si
counts / channel
pulse height channel
q18-phd-1 1
0
100
200
300
400
500
600
50
150
250

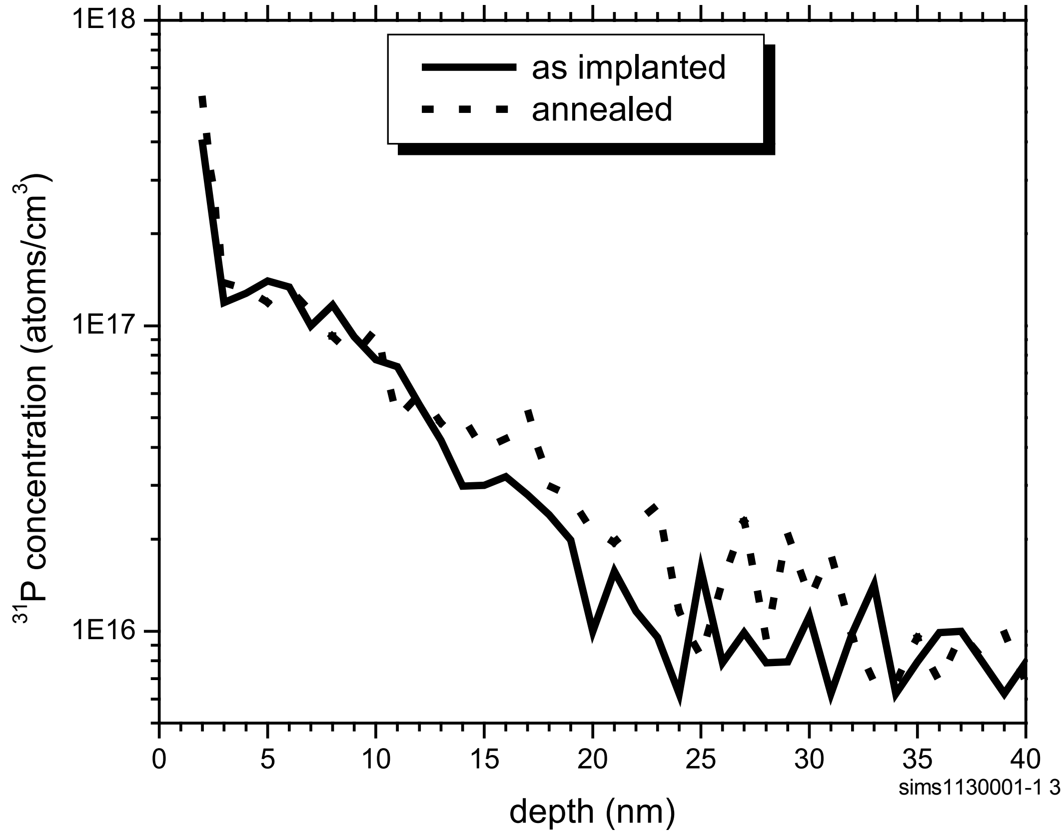

1E18
1E17
1E16
^{31}P concentration (atoms/cm^3)
as implanted
annealed
0
5
10
15
20
25
30
35
40
depth (nm)
sims1130001-1 3